HHS Public Access

Author manuscript

Nat Struct Mol Biol. Author manuscript; available in PMC 2018 April 30.

Published in final edited form as:

Nat Struct Mol Biol. 2017 December ; 24(12): 1064–1072. doi:10.1038/nsmb.3493.

Dissecting the telomere-inner nuclear membrane interface formed in meiosis

Devon F. Pendlebury[1,2], **Yasuhiro Fujiwara**[3], **Valerie M. Tesmer**[1], **Eric M. Smith**[1,2], **Hiroki Shibuya**[4], **Yoshinori Watanabe**[3], and **Jayakrishnan Nandakumar**[1,2]

[1]Department of Molecular, Cellular, and Developmental Biology, University of Michigan, Ann Arbor, MI, USA

[2]Program in Chemical Biology, University of Michigan, Ann Arbor, MI, USA

[3]University of Tokyo, Institute of Molecular and Cellular Biosciences, Laboratory of Chromosome Dynamics, Tokyo, Japan

[4]Department of Chemistry and Molecular Biology, University of Gothenburg, Gothenburg, Sweden

Abstract

Tethering telomeres to the inner nuclear membrane (INM) allows for homologous chromosome pairing during meiosis. A meiosis-specific protein TERB1 binds the telomeric protein TRF1 to establish telomere-INM connectivity and is essential for mouse fertility. Here we solve the structure of the human TRF1-TERB1 interface to reveal the structural basis for telomere-INM linkage. Disruption of this interface abrogates binding and compromises telomere-INM attachment in mice. An embedded CDK-phosphorylation site within the TRF1-binding region of TERB1 provides a mechanism for cap exchange, a late-pachytene phenomenon involving the dissociation of the TRF1-TERB1 complex. Indeed, further strengthening this interaction interferes with cap exchange. Finally, our biochemical analysis implicates distinct complexes for telomere-INM tethering and chromosome end protection during meiosis. Our studies unravel the structure, stoichiometry, and physiological implications underlying telomere-INM tethering, thereby providing unprecedented insights into the unique function of telomeres in meiosis.

Correspondence to: Jayakrishnan Nandakumar.

Author Contributions. J.N., D.F.P., V.M.T., and Y.W. designed experiments; D.F.P., V.M.T., E.M.S., and J.N. conducted the crystallographic experiments; D.F.P. conducted cloning, protein purifications, and *in vitro* binding studies; Y.F. conducted *in vivo* cellular localization studies with guidance from H.S.; J.N., D.F.P., and Y.W. analyzed the data; and J.N. and D.F.P. wrote the manuscript with input from all authors.

Competing financial interests statement. The authors declare no competing financial interests.

Data availability statement. Accession codes: Coordinates and structure factors have been deposited in the Protein Data Bank with accession code 5WIR. A Life Sciences Reporting Summary for this article is available online.
Source data associated with Figures 1, 2, 3, and 4 are available with the paper online. Other data accompanying this study are available upon request.

Introduction

Telomeres are nucleoprotein complexes found at chromosome ends that play a critical role in maintaining genome stability. Mammalian telomeres are composed of tandem DNA repeats of GGTTAG/CCAATC sequence ending with a 3′ guanosine-rich single strand overhang [1,2]. Mammalian telomeric DNA is coated with many copies of shelterin, a six-protein complex, consisting of TRF1, TRF2, TPP1, POT1, TIN2 and Rap1 [3]. TRF1 and TRF2 are the two double-stranded telomeric DNA-binding proteins within shelterin [4-6]. By binding specifically and with high affinity to telomeric DNA, shelterin performs multiple critical functions. First, shelterin protects telomeric DNA from being inappropriately recognized as a double strand break [3]. Second, shelterin is critical for the recruitment of the reverse transcriptase telomerase, which replicates the extreme ends of chromosomes [7].

In cells undergoing meiosis to produce haploid gametes for sexual reproduction [8,9], shelterin must fulfill a third, critical function. Specifically, telomeres attach to the inner nuclear membrane (INM) in meiotic prophase I. The LINC complex [10-12], consisting of SUN-domain and KASH-domain proteins, is important for linking chromosomes to the cytoskeletal motors, which enable chromosomal movement along the membrane [13-18]. This telomere-INM connection is thought to be important in enabling the proper pairing of homologous chromosomes and subsequent recombination. The recombination events are critical for producing genetic variation and important for ensuring proper segregation of homologous chromosomes during the first meiotic metaphase. While Bqt1 and Bqt2 proteins are involved in telomere-INM tethering in *S.pombe*, the Ndj1 protein performs a similar function in *S.cerevisiae* [19,20]. In contrast, the corresponding mammalian proteins cannot be detected using sequence-based homology searches.

Nevertheless, the recent identification of genes that are specifically expressed in mouse tissues undergoing meiosis by Shibuya et al. has led to the discovery of genes responsible for INM tethering of telomeres in mammals. The protein encoded by one of these genes, the TERB1 protein (telomere repeats-binding bouquet-formation protein) [21], is conserved amongst vertebrates and essential for fertility in mice. TERB1 protein is expressed only during meiotic prophase I, where it colocalizes with telomeres. *Terb1*$^{-/-}$ mice showed impaired meiosis due to loss of synapsis, lack of homologous chromosome pairing, and reduced chromosome movement during meiotic prophase I. These studies showed the importance of TERB1 protein for connecting telomeres to the cellular machinery via the nuclear membrane [21]. TERB1 protein was shown to directly interact with the shelterin component TRF1. The C-terminus of TERB1 (TRF1 binding domain or TERB1^{TRFB}; aa 523-656 for human TERB1) and the dimerization domain of TRF1 (TRF homology domain or TRF1^{TRFH}; aa 62-265 for human TRF1) are necessary and sufficient for this interaction [21]. TERB2 and MAJIN are two other meiotic telomere-INM proteins that were subsequently discovered [22,23]. TERB2 forms a stable complex with TERB1 and links it to MAJIN, which is anchored to the INM (Fig. 1a). Tethering of telomeres to the INM is followed by an intriguing phenomenon coined telomere cap exchange that occurs late in pachytene. During cap exchange, shelterin dissociates from its meiotic binding partners, resulting in a central TERB1-TERB2-MAJIN focus at telomeres surrounded peripherally by a more diffused shelterin signal [22]. Despite the recent mapping of the interactions that

connect telomeres to the INM (Fig. 1a), the structural basis for telomere-INM tethering remains completely unknown. How TRF1-TERB1 binding is switched on for initial INM attachment in early prophase I, and then off during cap exchange later in prophase I, is also poorly understood. Here we use a combination of X-ray crystallography, quantitative biochemistry, mouse meiosis models, and high-resolution microscopy of telomere-INM complexes to answer these critical questions in mammalian meiosis.

Results

TERB1 uses a variation of the strategy employed by TIN2 to bind TRF1

We noted that the CDK-consensus motif in the TERB1^{TRFB} domain [21], ^{648}TPRR^{651} [(S/T)PX(K/R)], overlaps with a sequence that resembles the “FXLXP” TRFH-binding motif (TBM) that TIN2 (^{258}FNLAP^{262} in TIN2) uses to bind TRF1 [24] (Fig. 1a). ^{645}ILLTP^{649} of TERB1 satisfies the FXLXP consensus sequence barring the presence of an F→I substitution. The characteristic “arginine tail” C-terminal to the FXLXP motif in TIN2 is also present in TERB1^{TBM} (TERB1 aa 643-656; Fig. 1a). Knowing also that the TERB1^{TRFB} domain is sufficient to bind TRF1 [21,22], we hypothesized that TERB1 binds TRF1 using a TBM. Indeed GST-hTERB1^{TBM} efficiently pulls down TRF1^{TRFH} (Fig. 1b).

To determine the structural basis for the TRF1-TERB1 interaction, we crystallized and solved the structure of the hTERB1^{TBM} - TRF1^{TRFH} complex to 2.1 Å (Table 1). The structure revealed two TERB1^{TBM} peptides bound to the two monomers of a TRF1^{TRFH} homodimer (Fig. 1c; Supplementary Fig. 1a and b). Next, we compared the interactions of TERB1 and TIN2 with TRF1 side-by-side based on the new TRF1^{TRFH} – TERB1^{TBM} structure and the previously reported TRF1^{TRFH} – TIN2^{TBM} structure [24]. TIN2 F258 binds a pocket of TRF1 lined by hydrophobic residues (center and right panels; Fig. 1d). In sharp contrast, the equivalent TERB1 I645 residue is mostly excluded from this pocket (Fig. 1d and h). Interestingly, TERB1 L646, which occupies a variable position in the (F/I)XLXP motif, partially occupies this hydrophobic pocket of TRF1 (Fig. 1d). The conserved LXP motif of TERB1 and TIN2 adopts very similar conformations in both structures (Fig. 1e and h). Finally, while the second arginine of the TRF1-binding motif in TIN2 (^{265}RRR^{267}) makes several important interactions with TRF1, it is the third arginine in this motif of TERB1 (^{650}RRR^{652}) that occupies a similar spatial position and participates in the equivalent interactions (Fig. 1f and h).

Our structure reveals the mechanism by which CDK phosphorylation of TERB1 T648 blocks binding of TERB1 to TRF1, thereby releasing telomeres from their tether at the INM in late pachytene [21]. The close proximity of the side-chains of TERB1 T648 and TRF1 E106 (3.0 Å; Fig. 1g) suggests that phosphorylation of TERB1 T648 (PO_4-**T648)** would result in electrostatic repulsion between two negatively charged residues, leading to the disruption of the binding interface. Overall our structural analysis of the TRF1-TERB1 interaction revealed an interface similar to, but less intimate than, the interface formed between TIN2 and TRF1.

Biochemical and biophysical validation of the TERB1-TRF1 interface

We performed GST pull down experiments using GST-TRF1^{TRFH} as bait and His-Smt3-tagged TERB1^{TBM} wild-type (WT) or mutant constructs as prey. While GST-TRF1^{TRFH} pulled down TERB1^{TBM} WT, I645E, L647E, T648E (phosphomimetic mutation), P649E, and R652E mutations of TERB1 ^{645}ILLTPRRR^{652} resulted in a complete loss of pull down (Supplementary Fig. 2a). We asked how replacing TERB1 I645 with a phenylalanine residue to create an FXLXP (^{645}FLLTP^{649}) motif affected TRF1 binding. Indeed, TERB1^{TBM} I645F was pulled down by TRF1^{TRFH} to at least WT levels (Supplementary Fig. 2a). The F142 residue of TRF1 stacks against the proline in the (F/I)XLXP motif of TERB1 (or TIN2; Fig. 1e). Consistent with our crystal structure and previous results with TIN2^{TBM} [24], the TRF1 F142A mutation abrogated TERB1^{TBM} binding (Supplementary Fig. 2b).

We quantified the importance of individual TRF1-TERB1 interactions using a flow cytometry protein interaction assay (FCPIA) technique that has been previously described [25]. The TRFH domain of TRF1 was biotinylated on cysteines with biotin maleimide and immobilized on uniformly sized spherical streptavidin beads (see Methods). The beads were incubated in the presence of increasing concentrations of GST-TERB1^{TBM} labeled with Alexa Fluor 488-maleimide (which reacts with cysteine sulfhydryl groups, only present on GST) and the median fluorescence of beads was analyzed by a flow cytometer. We determined a dissociation constant (K_d) of 75.1 ± 9 nM for the TRF1^{TRFH} – TERB1^{TBM} interaction (Fig. 1i). In contrast, TRF1^{TRFH} – TIN2^{TBM} binding was much stronger (K_d = 5.3 ± 1.2 nM; Fig. 1i), consistent with the more elaborate TRF1-TIN2 interface revealed by our structural analysis (Fig. 1d). We designed a competition experiment to quantitatively assess the TRF1-binding properties of TERB1^{TBM} mutants in the absence of labeling artifacts. For this, Alexa Fluor 488-labeled TERB1^{TBM} was pre-bound to TRF1^{TRFH} immobilized beads and the fluorescence was measured as a function of titrated unlabeled TERB1^{TBM} WT or mutant peptides. As in direct binding assays, TIN2^{TBM} was a more efficient competitor than TERB1^{TBM} WT protein (Fig. 1j; Supplementary Fig. 3a; Table 2). Additionally, TERB1^{TBM} I645E, L647E, T648E, P649E, and R652E were all severely impaired in their ability to displace WT TERB1 (Fig. 1j; Supplementary Fig. 3a; Table 2; statistics were derived from biological duplicates of means from technical duplicates). Indeed the TERB1 I645F mutation increased binding to TRF1^{TRFH} by ~3-fold compared to TERB1 WT (Fig. 1j; Supplementary Fig. 3a; Table 2).

To validate the importance of the TRF1-TERB1 interface in a more biologically relevant context, we co-expressed and purified a minimal TERB1-TERB2 complex, TERB1^{TRFB} - TERB2$^{1-107}$ (Supplementary Fig. 3c-f), based on domain definitions described for the corresponding complex in mice [22]. Competition analysis revealed that TERB1^{TRFB} – TERB2$^{1-107}$ WT showed a ~2-fold increase in affinity for TRF1 than TERB1^{TBM}, suggesting that while the TBM of TERB1 provides a large amount of the binding interface, structural determinants outside this region may also contribute to TRF1 binding (Fig. 1k; Supplementary Fig. 3b; Table 2). As with mutant TERB1^{TBM} peptides (Fig. 1j; Supplementary Fig. 3a), TERB1 I645E, L647E, and P649E mutations in the context of TERB1^{TRFB} - TERB2$^{1-107}$ drastically reduced binding affinity for TRF1^{TRFH}. Once again, the I645F displayed a moderate gain in binding affinity compared to WT (Fig. 1k;

Supplementary Fig. 3b; Table 2). These results demonstrate the importance of the TBM of TERB1 for TRF1 binding.

Disruption of the TERB1-TRF1 interface compromises inner nuclear membrane attachment of telomeres in prophase I of meiosis

We next tested the importance of the TRF1-TERB1 interface *in vivo*. We examined INM-telomere tethering in mouse *Terb1*$^{-/-}$ spermatocytes, which have been shown not to undergo synapsis and to arrest in either leptotene or zygotene-like stages. Accordingly, in zygotene-like *Terb1*$^{-/-}$ spermatocytes, the majority of TRF1-labeled telomeres remained detached from the nuclear membrane (Fig. 2a-c). This telomere attachment defect can be rescued with exogenously provided TERB1 WT (Fig. 2a-c) [21,22]. We attempted to rescue the *Terb1*$^{-/-}$ phenotype with TERB1^{TBM} mutants. Expression of I645E, L647E, T648D, and the R651E-R652E mouse TERB1 mutants showed a statistically significant defect in telomere attachment to the INM (Fig. 2b, c). Like TERB1 WT, mouse TERB1 I645F efficiently rescued the telomere attachment defect of the *Terb1*$^{-/-}$ spermatocytes (Fig. 2b, c). Taken together, we conclude that even single mutations in the TRF1-TERB1 interface can significantly reduce both binding *in vitro* and telomere-INM tethering *in vivo* (see summary in Supplementary Table 1), highlighting the importance of this interface in proper progression through meiosis.

Further reinforcing the TERB1-TRF1 interaction interferes with cap exchange in prophase I of meiosis

TRF1-TERB1 binding is critical for telomere attachment to the INM [21,22] in early pachytene (histone H1 variant H1T negative), but dissociation of this complex is necessary for telomere cap exchange later in pachytene [22] (H1T positive) (Fig. 3a). Upon cap exchange, shelterin proteins, including TRF1, are separated from the TERB1-TERB2-MAJIN complex producing a more diffuse signal [22]. Accordingly, the diameter of the TRF1 signals in late pachytene spermatocytes is greater than that in early pachytene spermatocytes (Fig. 3a, d, and schematic in panel e).

We hypothesized that separation of the meiosis-specific proteins from shelterin during cap-exchange is driven by weakening of the TRF1-TERB1 interaction. Indeed, CDK-mediated phosphorylation of TERB1, which we show would severely destabilize the TRF1-TERB1 interface, occurs during cap exchange [22]. Not surprisingly, expression of loss-of-binding TERB1 (I645E, L647E, P649E, and R651E/R652E), or TRF1 [F129A (equivalent of human TRF1 F142A)] mutants did not disrupt cap exchange in WT mouse spermatocytes (Fig. 3c, d; Supplementary Fig. 4b). To further test our hypothesis, we designed gain-of-function mutants to further strengthen the TRF1-TERB1 interaction. Human TRF1 E106 interacts with T648 and is expected to electrostatically repel TERB1 PO_4-T648 (Fig. 1g). We engineered the TRF1 E93K mutation (mouse TRF1 E93 is equivalent to human TRF1 E106) to create a positive charge suitable for interaction with TERB1 PO_4-T648. Intriguingly, GFP-TRF1 E93K expressed in late pachytene WT spermatocytes (H1T-positive) appeared as compact rather than diffused foci, whereas TRF1 E93A showed the normal diffused signal as WT (Fig. 3b, d). Remarkably, the diameter of the GFP-TRF1 E93K signal in late pachytene was unchanged relative to early pachytene (Fig. 3b, d). Because this experiment

was performed in wild-type mouse spermatocytes, we also tracked the localization of endogenous TRF1 relative to GFP-TRF1 E93K. Indeed endogenous TRF1 relocated to the periphery in late pachytene (Supplementary Fig. 5a), suggesting that barring interference by the E93K mutation, the cells are fully capable of undergoing normal cap exchange.

We also engineered mouse TERB1 I645F to further strengthen the TRF1-TERB1 interaction (Fig. 3c). The late pachytene GFP-TERB1 signal that is normally compact and separated from the diffused TRF1 signal (see WT or I645E), spread out to the periphery in the presence of the I645F mutation (Fig. 3c, e, and Supplementary Fig. 5b, c). We infer that the reinforced binding allows endogenous TRF1 to drag with itself (a subset of) TERB1 I645F molecules to the periphery despite CDK-dependent phosphorylation of TERB1. These data suggest that reinforcing the interaction between TRF1 and TERB1 proteins interferes with cap exchange *in vivo*.

TERB1 and TIN2 bind TRF1 in a mutually exclusive manner

Because TRF1 protein is known to be a homodimer, it is unclear whether TERB1 and TIN2 can simultaneously bind TRF1, or whether the binding of these proteins to TRF1 is mutually exclusive. If TRF1 were able to simultaneously bind TIN2 and TERB1, it would imply that the same shelterin complex can perform both INM tethering and chromosome end protection during meiosis. Our initial insights into this question came from the fluorescence-based competition assay already described. We pre-bound streptavidin beads-immobilized $TRF1^{TRFH}$ with Alexa Fluor 488-labeled $TERB1^{TBM}$ peptide. We then competed off this interaction using either full-length human TIN2 protein or the $TERB1^{TRFB}$ – $TERB2^{1\text{-}107}$ complex. We were surprised to observe that the height of the $TERB1^{TRFB}$ – $TERB2^{1\text{-}107}$ competition curve was roughly half that of the TIN2 competition curve (Fig. 4a; Supplementary Fig. 6a). Given that each TRFH domain in the homodimer binds one (TERB1 or TIN2) TBM peptide (Fig. 1c and Ref[24]), these results suggest that two copies of full-length TIN2 can fully displace the two TBM peptides from TRF1, but that only one TBM peptide is displaced by the $TERB1^{TRFB}$ – $TERB2^{1\text{-}107}$ protein complex (see schematic in Fig. 4a).

To further test this idea, we engineered a fusion protein encompassing two $TRF1^{TRFH}$ domains separated by a flexible glycine-serine linker. Using this system we engineered three intramolecular $TRF1^{TRFH}$ dimers: WT-WT (two TBM binding sites), WT-F142A (one TBM binding site), and F142A-F142A (no TBM binding sites; Fig. 4b; Supplementary Fig. 6b, c). Indeed TIN2 showed the expected increase in binding stoichiometry when bound to WT-WT versus WT-F142A (compare TIN2 stoichiometry in lanes 7 and 8 in Fig. 4c; replicate in Supplementary Fig. 6d; and statistics in Supplementary Fig. 6e). In contrast, TERB1-TERB2 did not show an increase in stoichiometry when binding WT-WT versus WT-F142A (compare $TERB1^{TRFB}$ and $TERB2^{1\text{-}107}$ stoichiometries in lanes 3 and 4 in Fig. 4c; replicate in Supplementary Fig. 6d; and statistics in Supplementary Fig. 6e). Thus we conclude that TERB1-TERB2 can occupy only one TBM-binding site in a TRF1 dimer. The vacancy in the second binding site of TRF1 when bound by TERB1-TERB2 may potentially be occupied by TIN2 to recruit other shelterin proteins for chromosome end protection. However, we failed to observe any TIN2 being pulled down on amylose beads containing

MBP-TERB1^{TRFB} - TRF1^{TRFH} (lane 6; Fig. 4d), suggesting that TRF1 is unable to simultaneously bind TIN2 and TERB1, at least in this experimental context.

Rap1 prevents binding of TERB1 to TRF2

It is known that TRF2 protein binds client proteins containing a YXLXP motif [24]. However TRF1, but not TRF2, was identified as a binding partner of TERB1 [21]. We asked how specificity for TRF1 versus TRF2 is achieved by TERB1. GST-TERB1^{TBM} pulls down TRF2^{TRFH} *in vitro* (Fig. 4f). Direct as well as competition experiments of human TRF2^{TRFH} versus TRF1^{TRFH} binding to TERB1^{TBM} revealed a roughly equal dissociation constant (K_d) of either TRF protein domain for TERB1^{TBM} peptide (TRF1^{TRFH}: 48 ± 8 nM; TRF2^{TRFH}: 42 ± 5 nM; Table 2; Supplementary Fig. 7a,b). However, competition analysis showed that TRF1^{TRFH} bound with greater affinity to the more physiologically relevant TERB1^{TRFB} – TERB2$^{1-107}$ complex versus the minimal TERB1^{TBM}, while the opposite trend was observed for TRF2^{TRFH} (Table 2). The TERB1-TRF2 interaction was also less specific than TRF1-TERB1 as TERB1 I645E and R652E mutations did not significantly affect TERB1-TRF2 binding (Supplementary Fig. 7c, d; Table 2).

The highly abundant TIN2 and Rap1 proteins of shelterin are known to associate with TRF2, although Rap1 is also involved in forming a higher-order complex with TRF2 (four subunits each of TRF2 and Rap1) [24,26,27]. Accordingly, we asked whether binding of TIN2 or Rap1 affects the TERB1-TRF2 interaction. Binding of TERB1 to TRF2 was severely hampered in the presence of Rap1 protein (Fig. 4g). Furthermore, ternary pull down experiments demonstrated that while MBP-TERB1^{TRFB} binds TRF2, it fails to do so in the presence of Rap1 (compare lanes 5 and 6; Supplementary Fig. 7e). A similar pull down experiment showed that TIN2 does not interfere with the TRF2-TERB1 interaction (Supplementary Fig. 7f). These results suggest that the association of TRF2 and Rap1 at telomeres possibly prevents a non-cognate TERB1-TRF2 interaction during meiosis.

Discussion

The unique role played by telomeres in meiotic cells raises several mechanistic questions with broad implications in both chromosome end biology and meiosis. First, how are telomeres anchored to the INM in early prophase I of meiosis? Here, we unravel the molecular architecture of the TERB1-TRF1 interface that orchestrates telomere attachment to the INM. Our structure shows that TERB1 uses an ILLTP-$(Arg)_3$ TBM motif to bind TRF1. A highly related FNLAP-$(Arg)_3$ TBM motif is used by TIN2 to recognize TRF1. However, the I residue in the binding motif of TERB1, unlike the F residue in TIN2, does not occupy a hydrophobic binding pocket in TRF1. Although TERB1 adapts the strategy used by TIN2 to bind TRF1, TIN2 is better able to exploit the binding surface available on TRF1. To validate our structural analysis, we performed both qualitative and quantitative binding experiments *in vitro*, as well as high-resolution protein-colocalization analysis *in vivo*. Combined, our results demonstrate that (i) TIN2 binds to TRF1 with higher affinity than TERB1 does; (ii) the TBM of TERB1 provides a large fraction of the binding interface with TRF1; and (iii) mutations in the L647, P649 and R652 residues in the TERB1 TBM drastically reduce binding to TRF1 and impair INM attachment of telomeres in *Terb1*$^{-/-}$

spermatocytes expressing TERB1 TBM-mutant proteins. However, we also note that none of the TERB1 mutants reduced telomere-INM tethering to the levels seen in *Terb1*$^{-/-}$ spermatocytes. This is probably because attachment of TERB1-TERB2-MAJIN to telomeres may involve binding to TRF1 of regions of TERB1 outside its TBM, as well as binding of MAJIN [22] and TERB1 [21] to telomeric DNA.

Second, how is the telomere-INM assembly rearranged during cap exchange? We wondered whether the variations in TERB1 TBM relative to TIN2 [F→I in (F/I)XLXP; and phosphorylation of TERB1 T648] are adaptations to attenuate the TERB1-TRF1 interaction for achieving cap exchange. Indeed the phosphomimetic mutation of T648 abrogated binding of TERB1 to TRF1 *in vitro*, and reduced telomere tethering to the INM ~15-fold relative to WT TERB1 *in vivo*. This is fully consistent with a highly unfavorable electrostatic repulsion between TERB1 PO_4-T648 and human TRF1 E106. We predicted that further reinforcing the TERB1-TRF1 interaction will compromise proper cap exchange. Indeed expression of gain-of-binding mutants mouse TRF1 E93K and mouse TERB1 I645F interfered with normal cap exchange. We conclude that the dynamic nature of the TERB1-TRF1 interaction in biology mandates an interface that is robust enough to initially anchor telomeres to the INM, but also malleable enough to allow dissociation as meiosis progresses. Furthermore, our observation that one but not both binding sites in a TRF1 dimer are available for binding TERB1 suggests yet another adaptation to facilitate TRF1-TERB1 dissociation during cap exchange.

Third, how is the meiosis-specific function of telomeres compatible with chromosome end protection in early and late pachytene? The interaction between TRF1 and TIN2 is essential for chromosome end protection by shelterin, as disruption of this interaction results in both ATR-mediated and ATM-mediated DNA damage response at telomeres [28,29]. Our binding experiments suggest that the end protection- and meiosis-specific functions of TRF1 are bestowed on separate pools of TRF1 protein. While TRF1 bound to TIN2 would perform normal end protection in early pachytene, this complex would not bind TERB1. Conversely, TRF1 bound to TERB1 would tether telomeres to the INM, but this TRF1 pool would be unable to bind TIN2 to assemble the rest of shelterin.

In late pachytene, one model is that TERB1/2-MAJIN takes over telomeric DNA by releasing the shelterin complex into a surrounding ring structure (cap exchange). In this window of the cell cycle, TERB1-TERB2-MAJIN may completely replace shelterin for performing end protection. However it is intriguing that shelterin, although not localized at telomeric DNA, is still in its immediate vicinity after cap exchange [22]. One explanation for how shelterin remains close to telomeric DNA without binding either DNA or TERB1 is that it phase-separates *en bloc* forming an oil-droplet like structure around it. Such condensates have been observed in various other biological contexts, including DNA damage response, RNA storage and stability, and ribosome biogenesis [30]. Another possibility is that TERB1-TERB2-MAJIN displaces shelterin from the extreme chromosome ends to internal (i.e., closer to centromeres) telomeric or sub-telomeric regions in late pachytene. Under such a setup, TERB1-TERB2-MAJIN and shelterin could share the burden of chromosome end protection. Finally, it is also possible that the spatial separation of complexes observed in cap exchange denote separation of TERB1-TERB2-MAJIN and shelterin on different

telomeric structures (e.g., t-loops) or chromatin states in late pachytene (rather than different loci on chromosomes). While shelterin will continue to protect chromosome ends as usual, TERB1-TERB2-MAJIN as part of altered telomeric structure/chromatin state might allow proper anchoring of the ends of chromosomes to the INM.

Fourth, how is specificity for TRF1 versus TRF2 established for TERB1? Our data provide multiple lines of evidence to suggest that the cognate binding partner of TERB1 is TRF1, not TRF2. (1) TRF1 but not TRF2 prefers binding to $TERB1^{TRFB}$ - $TERB2^{1\text{-}107}$ over $TERB1^{TBM}$ peptide, suggesting that TRF1 has adapted to bind TERB1 while TRF2 has not. (2) The TRF2-TERB1 interaction is less specific compared to the TRF1-TERB1 interaction, insofar as TRF2 binding is insensitive to certain mutations in the TERB1 TBM. (3) Binding of TERB1 to TRF2 is abrogated in the presence of Rap1, an abundant human shelterin protein [31] that binds strongly to TRF2 [32] and is present along with the rest of shelterin at meiotic telomeres [22].

In summary, our studies unravel a structural interface critical for tethering telomeres to the INM; validate its importance *in vivo*; define the rules guiding not just its formation but also its cell cycle-dependent dissociation in meiotic cells; and provide a rationale for how this interface is able to sustain chromosome end protection while simultaneously avoiding non-cognate interactions.

Online Methods

Primers, cDNA, and plasmid constructs

All primers were purchased from Integrated DNA Technologies (IDT). The pSmt3 vector used to generate His-Smt3 fusions in *E. coli* was obtained from Dr. Christopher D. Lima upon signing a material transfer agreement with Cornell University, New York [33]. Co-expression of recombinant proteins in *E. coli* was performed using the pET-Duet vector (Novagen). For expression in baculovirus-infected insect cells, the expression constructs were cloned into the pFastbac vector (Life Technologies) encoding an N-terminal His-Sumostar tag (Lifesensors). pSmt3-TERB1-523-656 (for $TERB1^{TRFB}$ protein) and pSmt3-TERB1-643-656 (for $TERB1^{TBM}$ peptide) were generated by PCR amplifying the sequences from hTERB1 cDNA (gene block; IDT). PCR inserts post-restriction digestion were ligated into pSmt3 vector using BamHI (New England Biolabs; NEB) and XhoI sites (NEB). A hTERB2 cDNA clone was obtained from GE Healthcare/Dharmacon (clone: MHS6278-202809054) and the sequence encoding residues 1-107 was amplified by PCR, cloned into the pSmt3 vector as described for TERB1. For co-expression experiments, $hTERB1^{TRFB}$ and $hTERB2^{1\text{-}107}$ sequences were cloned into the pET-Duet vector (Novagen) with TERB1 harboring a 10X-His-Smt3 tag and TERB2 expressed without a tag. $TRF1^{TRFH}$ and $TRF2^{TRFH}$, and full-length TRF2 were amplified from cDNA and cloned into the pSmt3 vector. Full-length TIN2 and Rap1 coding regions were amplified from cDNA and cloned into the pSumostar-Fastbac vector backbone for expression in High Five insect cells (Life Technologies). For GST-tagged and His-Smt3-MBP-tagged constructs, BamHI/XhoI double-digested inserts were ligated into the pGEX-6P-2 vector (GE Life Sciences) and the pSmt3-MBP vector (derived by cloning the MBP cDNA into pSmt3), respectively. Intramolecular $TRF1^{TRFH}$ homodimeric constructs were cloned in the pSmt3 vector using two, tandem

TRF1^{TRFH} cDNA sequences separated in-frame by DNA sequence coding for a 5 amino acid gly/ser linker.

Site-directed mutagenesis of plasmids

Mutations in both TERB1 and TRF1 expression plasmids were introduced using the QuikChange Site-Directed Mutagenesis kit (Agilent Technologies) and complementary mutagenic primers (Integrated DNA Technologies). Sanger sequencing was used to confirm the presence of the intended mutation and absence of unwanted sequence changes introduced during the cloning process.

Protein expression and purification

WT and mutant constructs of His-Smt3-TRF1^{TRFH}, His-Smt3-TRF2^{TRFH}, GST-TRF1^{TRFH}, GST-TRF2^{TRFH}, GST-TERB1^{TBM}, and TRFH intramolecular dimers were expressed in BL21(DE3) cells; and His-Smt3-TERB1^{TBM}, His-Smt3-TERB1^{TRFB} - TERB2$^{1-107}$, and His-MBP-Smt3-TERB1^{TRFB} were expressed in Rosetta(DE3) codon supplemented cells. Expression of recombinant proteins in *E. coli* was induced with isopropyl β-d-thiogalactopyranoside. Nickel-agarose affinity chromatography was used as the first step of purification of His-Smt3-tagged proteins. His-Smt3-TERB1^{TBM} WT and mutant proteins used for pull downs and binding studies were not subjected to removal of the Smt3 tag. All other Smt3 fusions were cleaved with Ulp1 protease to remove the His-Smt3 tag, and purified further using size-exclusion chromatography (Superdex 75 for proteins/complexes < 50 kDa and Superdex 200 for proteins/complexes > 50 kDa; GE Healthcare). Full-length human TIN2 and Rap1 proteins were expressed in baculovirus-infected High Five insect cells (Life Technologies) as His-Sumostar fusion proteins using the manufacturer's protocol. Subsequent purification was performed as described for Smt3-tagged proteins with the exception that Sumostar protease (Lifesensors) was used to cleave the His-Sumostar tag. Anion-exchange (HiTrap Q; GE Healthcare) was performed as the final polishing step of purification of Rap1 and TIN2. GST-tagged proteins were purified using Glutathione Sepharose 4B beads (GE Healthcare) following the manufacturer's instructions. TERB1 643-656 used for crystallography, after removal of the His-Smt3 tag, was purified further via size exclusion chromatography (Superdex 75; GE Healthcare) in 100 mM ammonium bicarbonate buffer, lyophilized, and resuspended in water before being subjected to co-crystallization with TRF1^{TRFH}.

Pull down assays

For GST-glutathione beads pull down experiments, 30 μl of a 1:1 slurry of Glutathione Sepharose 4B beads (GE Healthcare) pre-washed three times with binding buffer [25 mM Tris-Cl (pH 8.0), 150 mM NaCl, and 2 mM 2-mercaptoethanol] was incubated with 20 μg of GST-tagged bait protein for 1 hour at 4°C. 20 μg of prey protein was then added and incubation continued for 1 h at 4°C. The beads were then washed three times with binding buffer and heated at 95°C for 10 min in denaturing SDS gel-loading dye. The proteins were resolved on a 15% SDS-PAGE gel and visualized with Coomassie blue stain. MBP-Amylose beads pull down experiments were performed similarly, but with Amylose Resin High Flow (NEB) and MBP-tagged bait proteins. Quantitation of coomassie-stained SDS-PAGE pull down data was performed using the ImageJ software. In all cases, background-corrected

band intensities were divided by the molecular weight of the species followed by normalization against the molecular weight-normalized intensity of the bait protein in that lane.

Flow-cytometry based assay for quantifying protein-protein interactions

Direct binding experiments: Proteins were typically labeled as described in Blazer et al [25]. Specifically, we reacted a 2-5 fold excess of label over protein concentration for half an hour at room temperature. Unreacted label was removed with a Micro Bio-spin 6 spin column (Bio-Rad) and protein concentration was measured by the Protein Assay Reagent (Bio-Rad). The bait protein was biotinylated using biotin maleimide (Sigma; B1267) and immobilized on uniformly-sized streptavidin beads (Spherotech; SVP-20-5). 6 μl beads were used for an entire 96 well plate. The prey protein was fluorophore-labeled at cysteine residues (Alexa Fluor488-C5-maleimide, Life Technologies) and varying concentrations of prey proteins were mixed with the bait protein on beads in a buffer containing 20 mM Tris-Cl (pH 8.0), 100 mM NaCl, 2 mM DTT, 1% bovine serum albumin, and 0.1% lubrol. Upon equilibration on ice for 30 min, samples were loaded on an Accuri C6 flow cytometer (BD biosciences) using a Hypercyt autosampler (IntelliCyt). In every experiment, the median fluorescence intensity from each titration point was scored from approximately 500-1500 beads using the flow cytometer. Median fluorescence intensity on the beads was calculated using the Hypercyt software for a technical duplicate from the same plate, and the obtained mean values of the duplicate measurements were fitted to a single site binding model and dissociation constant (K_d) values calculated using Prism 7.0 (Graphpad) after subtracting background data from the same experiment performed without any bait protein bound to beads. We treated each site in the TRF1 (or TRF2) homodimer as an independent site in our analysis because we did not observe binding profiles suggestive of cooperativity. We note that the direct binding technique used here potentially underestimates the binding affinity (i.e., overestimates K_d), because labeling at or close to the interface will likely reduce affinity. Direct binding experiments were performed either two or three times.

Competition experiments: The two interacting proteins were labeled with biotin and fluorophore, respectively, as in direct binding studies, and held at a constant concentration throughout the experiment. Competition analysis was performed using 30 nM Alexa Fluor 488-labeled GST-TERB1. The unlabeled competitor protein was titrated into this mixture, and fluorescence intensity measurements were conducted as already described except that incubation of binding mixtures prior to flow cytometry was performed for 1 h to ensure equilibration. Median fluorescence values were fitted to a one-site competition curve and IC_{50} values calculated in Prism 7.0 (Graphpad). Competition experiments were performed either two or three times.

Structure determination of the $TRF1^{TRFH}$-$TERB1^{TBM}$

$TRF1^{TRFH}$ and $TERB1^{TBM}$ were mixed in a 1:5 molar ratio and crystal screens set up using 0.3 μl protein solution and 0.3 μl reservoir solution in a sitting drop format. Diffracting crystals were obtained in 0.1 M Tris-Cl (pH 8.5) and 30% PEG 300. Crystals were cryoprotected in the crystallization solution plus 10% PEG 400 and harvested in liquid nitrogen. Diffraction data were collected at the LS-CAT beamline 21 ID-F at the Argonne

National Laboratory at 0.97872 nm wavelength and 100 K temperature, indexed and processed using Mosflm (CCP4i [34]), and scaled using Aimless (CCP4i). Molecular replacement was performed using Molrep (CCP4i) with the structure of the TRF1^{TRFH} domain (PDB: 3BQO) serving as a search model. Preliminary refinement of the molecular replacement solution was performed using REFMAC (CCP4i), and the model was built in Coot [35]. The final rounds of refinement were performed using Phenix [36]. The final structural model exhibited excellent geometry, and contained no residues in the disallowed regions of the Ramachandran plot. Figures depicting structures were prepared in Pymol (http://www.pymol.org/).

Animals

For telomere attachment analysis, *Terb1* knockout mice (*Terb1*$^{tm2a(KOMP)Mbp}$) on a C57BL/6J background [21] were used. For telomere cap exchange analysis, C57BL/6J mice were purchased from Japan SLC, Inc. (Shizuoka, Japan). Animal experiments complied with ethical regulations and were approved by the Institutional Animal Care and Use Committee (approval #2809). No statistical method was used to estimate sample size.

Antibodies for *in vivo* analysis

The following antibodies were used in the mouse studies: mouse antibody against TRF1 (1:2000 dilution; in-house) [21], chicken antibody against GFP (1:500 dilution, Abcam, ab13970), guinea pig antibody against H1t (1:500 dilution, courtesy Handel lab) [37], rat antibody against SYCP3 (1:200 dilution; in-house) [21].

Exogenous expression of TRF1 and TERB1 in mouse testis

Plasmid DNA was injected into live-mouse testes based on a previously reported method with some modifications [38]. Briefly, mice at 20 days post-partum (dpp) for WT mice and 30 dpp for *Terb1*$^{-/-}$ mice were anesthetized. 50 μg of plasmid DNA (10 μl of 5 μg/μl DNA solution) was injected into the rete testis using a glass capillary under a stereomicroscope. After 60 min, electric pulses were applied four times at 50 V for 50 ms at 950 ms intervals, and the same electric pulses were applied again in the reverse direction. The testes were then placed in the abdominal cavity. After 24 h or 72 h of electroporation for WT or *Terb1*$^{-/-}$ mice, respectively, the mice were euthanized. The testes were extracted and used for cell preparations as described below.

Immunostaining of mouse spermatocytes

We followed a procedure described previously with some modifications [22]. Briefly, seminiferous tubules were extracted from the testes and minced using forceps. Germ cells were collected by pipetting for 1-2 min, washed three times with PBS, and the collected cells were resuspended in hypotonic buffer [30 mM Tris-Cl (pH 7.5), 17 mM Tris-Sodium citrate, 5 mM EDTA, and 50 mM sucrose] for 5 min at RT. After centrifuging at 500 × g for 5 min, the cells were resuspended in fixation buffer (1.5% PFA, 0.1% Triton X-100, and 100 mM sucrose in PBS) and placed on glass slides for 6 h or overnight at RT. After fixation, the cells were air-dried and used for immunostaining. The cells were permeabilized by incubating the slides in 0.1% Triton X-100 in PBS for 15 min at RT, and washing twice with

PBS. For immunostaining, the slides were incubated with 5% BSA in PBS for 30 min at RT. First, the primary antibodies listed above were applied and the slides were incubated over night at RT, after which the slides were incubated with secondary antibodies conjugated with Alexa Fluor 488, 568 or 647 (Life Technologies) (1:500 dilution) for 2 h at RT. The slides were washed with PBS and mounted using VECTASHIELD mounting medium with DAPI (VECTOR Laboratories).

Microscopy of mouse spermatocytes

Images were obtained on an IX-70 microscope (Olympus) equipped with a Delta Vision core system (GE Healthcare) and a CoolSNAP HQ CCD camera (Roper Scientific). A total of 100-140 Z sections were acquired in 0.1 μm steps using Olympus 100x 1.35NA UPlanApo objectives. The images were deconvolved using softWoRx version 5.5.5 acquisition software (GE Healthcare), and stacked images were analyzed for measurements. The width and area of telomere signals were measured using Fiji software [39]. For visualization purposes, magnified pictures of telomeres were cropped from a stacked picture of selected sections containing the target telomere using Fiji software [39], and the contrast of the image was enhanced using Photoshop (Adobe).

Statistics for *in vivo* data

Kruskal-Wallis one-way analysis of variance (ANOVA) with Tukey-Kramer's multiple comparisons test was performed to estimate the differences among groups. Data were analyzed using GraphPad version 7.0a. All plots were made using R Studio version 0.98.1103 (The R Foundation for Statistical Computing).

Supplementary Material

Refer to Web version on PubMed Central for supplementary material.

Acknowledgments

We thank the Life Sciences Collaborative Access Team at Argonne National Laboratory beamline staff for help with X-ray data collection; M. Iyer for help with protein purifications and S. Grill for excellent feedback on the manuscript. This work was funded by NIH Grants R00CA167644 (to J.N.), R01GM120094 (to J.N.), R01AG050509 (to J.N.; co-investigator); American Cancer Society Research Scholar grant 130882-RSG-17-037-01-DMC (to J.N.), NIH Biology of Aging Training Grant (T32AG000114) awarded to the University of Michigan Geriatrics Center from the National Institute on Aging (fellowship to E.M.S.), and MEXT KAKENHI 25000014 (to Y.W.).

References

1. Blackburn EH. Switching and signaling at the telomere. Cell. 2001; 106:661–673. [PubMed: 11572773]
2. Makarov VL, Hirose Y, Langmore JP. Long G tails at both ends of human chromosomes suggest a C strand degradation mechanism for telomere shortening. Cell. 1997; 88:657–666. [PubMed: 9054505]
3. Palm W, de Lange T. How shelterin protects mammalian telomeres. Annu Rev Genet. 2008; 42:301–334. [PubMed: 18680434]
4. Bilaud T, Brun C, Ancelin K, Koering CE, Laroche T, Gilson E. Telomeric localization of TRF2, a novel human telobox protein. Nat Genet. 1997; 17:236–239. [PubMed: 9326951]

5. Broccoli D, Smogorzewska A, Chong L, de Lange T. Human telomeres contain two distinct Myb-related proteins, TRF1 and TRF2. Nat Genet. 1997; 17:231–235. [PubMed: 9326950]
6. Nishikawa T, Okamura H, Nagadoi A, Konig P, Rhodes D, Nishimura Y. Solution structure of a telomeric DNA complex of human TRF1. Structure. 2001; 9:1237–1251. [PubMed: 11738049]
7. Nandakumar J, Cech TR. Finding the end: recruitment of telomerase to telomeres. Nat Rev Mol Cell Biol. 2013; 14:69–82. [PubMed: 23299958]
8. Watanabe Y. Geometry and force behind kinetochore orientation: lessons from meiosis. Nat Rev Mol Cell Biol. 2012; 13:370–382. [PubMed: 22588367]
9. Marston AL, Amon A. Meiosis: cell-cycle controls shuffle and deal. Nat Rev Mol Cell Biol. 2004; 5:983–997. [PubMed: 15573136]
10. Scherthan H. A bouquet makes ends meet. Nat Rev Mol Cell Biol. 2001; 2:621–627. [PubMed: 11483995]
11. Scherthan H, Weich S, Schwegler H, Heyting C, Harle M, Cremer T. Centromere and telomere movements during early meiotic prophase of mouse and man are associated with the onset of chromosome pairing. J Cell Biol. 1996; 134:1109–1125. [PubMed: 8794855]
12. Hiraoka Y, Dernburg AF. The SUN rises on meiotic chromosome dynamics. Dev Cell. 2009; 17:598–605. [PubMed: 19922865]
13. Sato A, Isaac B, Phillips CM, Rillo R, Carlton PM, Wynne DJ, Kasad RA, Dernburg AF. Cytoskeletal forces span the nuclear envelope to coordinate meiotic chromosome pairing and synapsis. Cell. 2009; 139:907–919. [PubMed: 19913287]
14. Conrad MN, Lee CY, Chao G, Shinohara M, Kosaka H, Shinohara A, Conchello JA, Dresser ME. Rapid telomere movement in meiotic prophase is promoted by NDJ1, MPS3, and CSM4 and is modulated by recombination. Cell. 2008; 133:1175–1187. [PubMed: 18585352]
15. Koszul R, Kim KP, Prentiss M, Kleckner N, Kameoka S. Meiotic chromosomes move by linkage to dynamic actin cables with transduction of force through the nuclear envelope. Cell. 2008; 133:1188–1201. [PubMed: 18585353]
16. Scherthan H, Wang H, Adelfalk C, White EJ, Cowan C, Cande WZ, Kaback DB. Chromosome mobility during meiotic prophase in Saccharomyces cerevisiae. Proc Natl Acad Sci U S A. 2007; 104:16934–16939. [PubMed: 17939997]
17. Trelles-Sticken E, Adelfalk C, Loidl J, Scherthan H. Meiotic telomere clustering requires actin for its formation and cohesin for its resolution. J Cell Biol. 2005; 170:213–223. [PubMed: 16027219]
18. Ding X, Xu R, Yu J, Xu T, Zhuang Y, Han M. SUN1 is required for telomere attachment to nuclear envelope and gametogenesis in mice. Dev Cell. 2007; 12:863–872. [PubMed: 17543860]
19. Chikashige Y, Tsutsumi C, Yamane M, Okamasa K, Haraguchi T, Hiraoka Y. Meiotic proteins bqt1 and bqt2 tether telomeres to form the bouquet arrangement of chromosomes. Cell. 2006; 125:59–69. [PubMed: 16615890]
20. Conrad MN, Dominguez AM, Dresser ME. Ndj1p, a meiotic telomere protein required for normal chromosome synapsis and segregation in yeast. Science. 1997; 276:1252–1255. [PubMed: 9157883]
21. Shibuya H, Ishiguro K, Watanabe Y. The TRF1-binding protein TERB1 promotes chromosome movement and telomere rigidity in meiosis. Nat Cell Biol. 2014; 16:145–156. [PubMed: 24413433]
22. Shibuya H, Hernandez-Hernandez A, Morimoto A, Negishi L, Hoog C, Watanabe Y. MAJIN Links Telomeric DNA to the Nuclear Membrane by Exchanging Telomere Cap. Cell. 2015; 163:1252–1266. [PubMed: 26548954]
23. Shibuya H, Watanabe Y. The meiosis-specific modification of mammalian telomeres. Cell Cycle. 2014; 13:2024–2028. [PubMed: 24870409]
24. Chen Y, Yang Y, van Overbeek M, Donigian JR, Baciu P, de Lange T, Lei M. A shared docking motif in TRF1 and TRF2 used for differential recruitment of telomeric proteins. Science. 2008; 319:1092–1096. [PubMed: 18202258]
25. Blazer LL, Roman DL, Muxlow MR, Neubig RR. Use of flow cytometric methods to quantify protein-protein interactions. Current protocols in cytometry. 2010; Chapter 13 Unit 13 11 11-15.
26. Li B, Oestreich S, de Lange T. Identification of human Rap1: implications for telomere evolution. Cell. 2000; 101:471–483. [PubMed: 10850490]

27. Arat NO, Griffith JD. Human Rap1 interacts directly with telomeric DNA and regulates TRF2 localization at the telomere. J Biol Chem. 2012; 287:41583–41594. [PubMed: 23086976]
28. Frescas D, de Lange T. Binding of TPP1 Protein to TIN2 Protein Is Required for POT1a,b Protein-mediated Telomere Protection. J Biol Chem. 2014; 289:24180–24187. [PubMed: 25056954]
29. Takai KK, Kibe T, Donigian JR, Frescas D, de Lange T. Telomere protection by TPP1/POT1 requires tethering to TIN2. Mol Cell. 2011; 44:647–659. [PubMed: 22099311]
30. Banani SF, Lee HO, Hyman AA, Rosen MK. Biomolecular condensates: organizers of cellular biochemistry. Nat Rev Mol Cell Biol. 2017; 18:285–298. [PubMed: 28225081]
31. Takai KK, Hooper SM, Blackwood SL, Gandhi R, de Lange T. In vivo stoichiometry of shelterin components. J Biol Chem. 2009; 285:1457–1467. [PubMed: 19864690]
32. Janouskova E, Necasova I, Pavlouskova J, Zimmermann M, Hluchy M, Marini V, Novakova M, Hofr C. Human Rap1 modulates TRF2 attraction to telomeric DNA. Nucleic Acids Res. 2015; 43:2691–2700. [PubMed: 25675958]

Methods-only References

33. Mossessova E, Lima CD. Ulp1-SUMO crystal structure and genetic analysis reveal conserved interactions and a regulatory element essential for cell growth in yeast. Mol Cell. 2000; 5:865–876. [PubMed: 10882122]
34. CCP4 (Collaborative Computational Project, N. The CCP4 suite: programs for protein crystallography. Acta Crystallogr D Biol Crystallogr. 1994; 50:760–763. [PubMed: 15299374]
35. Emsley P, Cowtan K. Coot: model-building tools for molecular graphics. Acta Crystallogr D Biol Crystallogr. 2004; 60:2126–2132. [PubMed: 15572765]
36. Adams PD, et al. PHENIX: a comprehensive Python-based system for macromolecular structure solution. Acta Crystallogr D Biol Crystallogr. 2010; 66:213–221. [PubMed: 20124702]
37. Cobb J, Cargile B, Handel MA. Acquisition of competence to condense metaphase I chromosomes during spermatogenesis. Developmental biology. 1999; 205:49–64. [PubMed: 9882497]
38. Shibuya H, Morimoto A, Watanabe Y. The dissection of meiotic chromosome movement in mice using an in vivo electroporation technique. PLoS Genet. 2014; 10:e1004821. [PubMed: 25502938]
39. Schindelin J, et al. Fiji: an open-source platform for biological-image analysis. Nature methods. 2012; 9:676–682. [PubMed: 22743772]

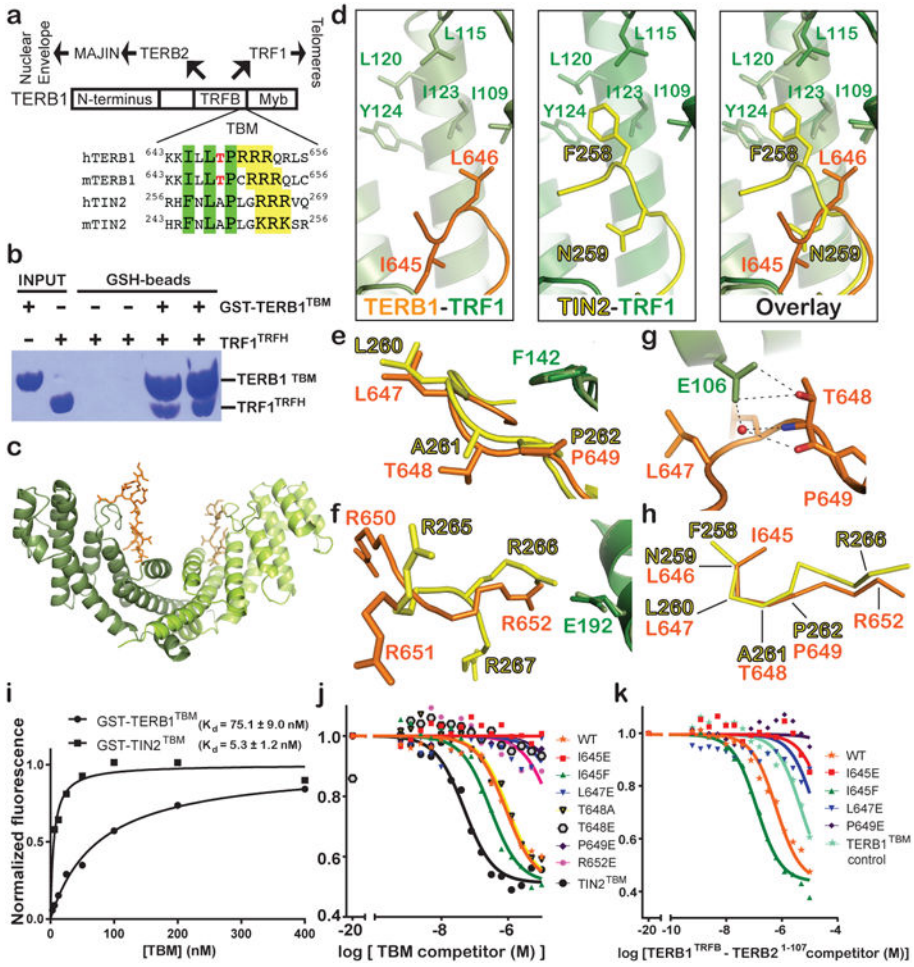

Figure 1. Structural and biochemical dissection of the TRF1^{TRFH} - TERB1^{TBM} interface

(a) Domain diagram of human TERB1 is shown along the connectivities from the telomere to the inner nuclear membrane. Alignment of the TBM motifs of human and mouse, TERB1 and TIN2, are shown below the domain diagram. (b) Pull down of TRF1^{TRFH} using GST-TERB1^{TBM} peptide (done in duplicate) on glutathione (GSH) sepharose beads as bait. Experiment was performed twice. (c) Overall structure of TRF1^{TRFH} - TERB1^{TBM} is shown with the TRF1 subunits (green) and the two bound TERB1^{TBM} peptides (orange) rendered in ribbon and stick representations, respectively. (d) Comparison of the interactions of the (I/F)X residues of TERB1 (*left*) and TIN2 (*center*) with TRF1^{TRFH}; the *right* panel shows a superposition of the two structures. (e) Overlay of TIN2^{TBM} (yellow) and TERB1^{TBM} (orange) bound TRF1^{TRFH} (green) structures showing a similar conformation adopted by the LXP residues of TERB1 and TIN2. (f) Overlay of TERB1^{TBM} and TIN2^{TBM} bound TRF1^{TRFH} structures showing the different conformation adopted by the tri-arginine stretch. (g) Binding of TERB1 to TRF1^{TRFH} places the CDK-phosphorylation site TERB1 T648 in close proximity to the negatively charged TRF1 E106; the red sphere indicates a water molecule bridging these residues using H-bonding. (h) Overlay of the TERB1^{TBM} versus TIN2^{TBM} peptide backbone segments from their respective TRF1^{TRFH}-bound structures. (i) Direct association of Alexa Fluor 488-labeled GST-TERB1^{TBM} or GST-TIN2^{TBM} with biotin-labeled TRF1^{TRFH} on streptavidin beads was scored with a flow cytometer. The

fluorescence signal was background corrected with binding reactions using unbound streptavidin beads. Mean of technical duplicate is plotted. Mean and s.e.m. values are indicated. Experiment was performed twice. (j-k) Fluorescence-based competition experiments using Alexa Fluor 488-labeled GST-TERB1^{TBM} (30 nM) pre-bound to biotin-labeled TRF1^{TRFH} on streptavidin beads titrated with varying concentrations of the indicated unlabeled TERB1^{TBM} peptides (j) or TERB1^{TRFB} – TERB2$^{1\text{-}107}$ complexes (k). Mean of technical duplicate is plotted. Mean and s.e.m. of two biological replicates (of technical duplicates) are shown in Table 2.

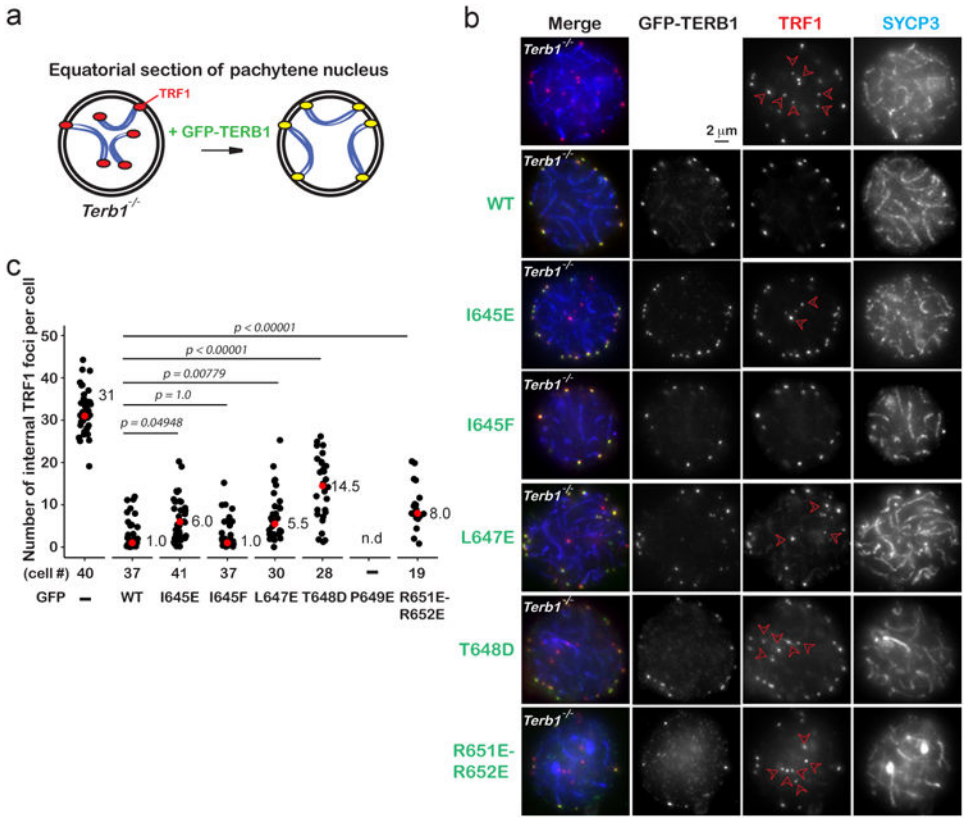

Figure 2. Weakening the TRF1-TERB1 interface compromises telomere-INM tethering

(a) Schematic showing telomere-INM attachment defect in *Terb1*$^{-/-}$ pachytene cells that can be rescued with GFP-TERB1 WT expression. (b) Equator images of *Terb1*$^{-/-}$ pachytene-like mouse spermatocytes expressing GFP-TERB1 WT, GFP-TERB1 I645E, GFP-TERB1 I645F, GFP-TERB1 L647E, GFP-TERB1 T648D, GFP-TERB1 P649E, or GFP-TERB1 R651E-R652E (green) stained with TRF1 (red) and SYCP3 (blue) antibodies. Red arrowheads indicate internal TRF1 foci. (c) Graph showing the number of internal TRF1 foci (black dot) in each cell with the median indicated (red dot). Only cells expressing a relatively strong GFP-TERB1 signal intensity were scored in this assay. Statistical significance (*P*-values) was assessed by one-way analysis of variance (ANOVA) with Tukey-Kramer's multiple comparisons test relative to GFP-WT. The numbers below indicate the number of cells observed.

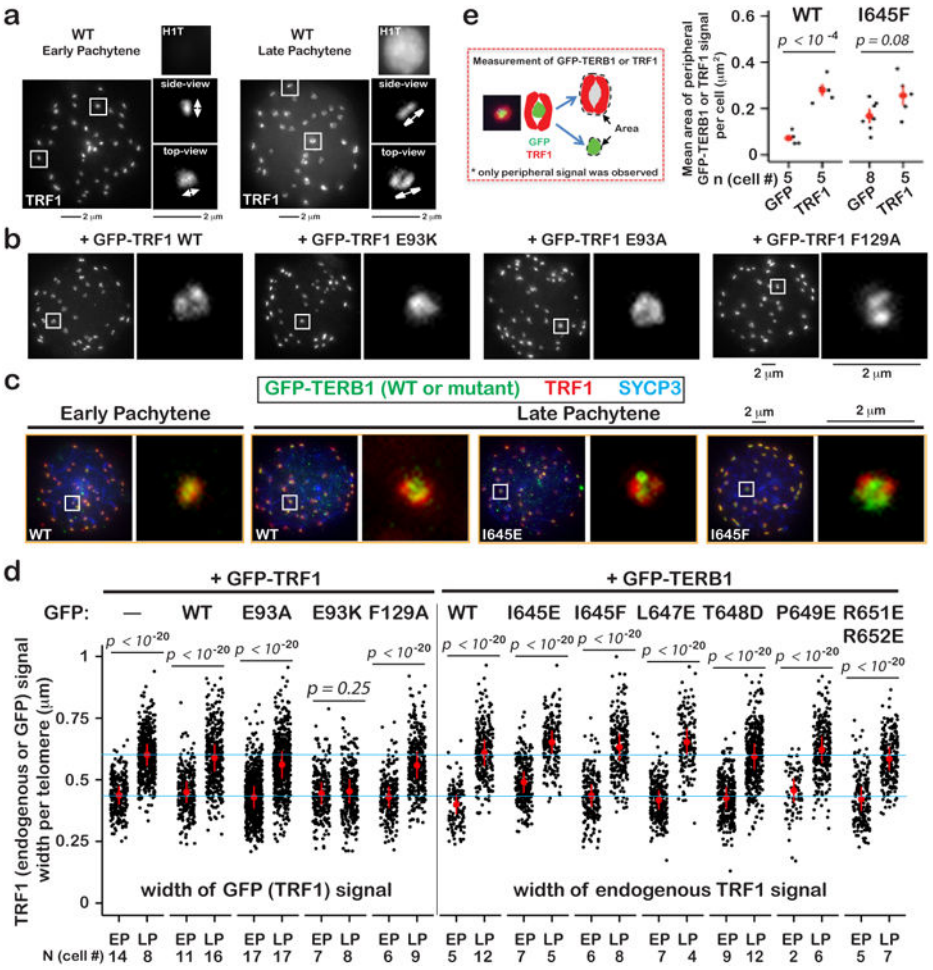

Figure 3. Further strengthening the TRF1-TERB1 interface disrupts cap exchange

(a) Projection images of WT early pachytene (*left*, H1T-negative) and late pachytene (*right*, H1T-positive) spermatocytes stained with TRF1 antibody. Equator and peripheral images of telomere-localized TRF1 (white rectangles) are shown in magnified views. Double-ended arrows indicate the outer diameter of the TRF1 signal. (b) WT spermatocytes in late pachytene expressing GFP-TRF1 WT, GFP-TRF1 E93K, GFP-TRF1 E93A, or GFP-TRF1 F129A. Magnified images of synapsed telomeres at the nuclear peripheries (white rectangles) are shown. (c) WT spermatocytes expressing GFP-TERB1 WT, GFP-TERB1 I645E, or GFP-TERB1 I645F (green) stained with TRF1 (red) and SYCP3 (blue) antibodies at the indicated stage of pachytene. (d) Graph showing the diameter of GFP-TRF1 or endogenous TRF1 signals of each telomere (black dot) with the mean (red dot) and s.d. (red bar). For cells expressing GFP-TRF1, the outer diameter of the GFP signal was measured, and for control cells and cells expressing GFP-TERB1, the outer diameter of the endogenous TRF1 signal was measured. The numbers below indicate the number of cells observed. Blue lines indicate the average outer diameter of the TRF1 signals in early pachytene (EP) or late pachytene (LP) spermatocytes. *P*-values for the early/late pachytene pairs for each TRF1 or TERB1 construct are indicated above the plot. (e) Schematic shows method for determining the area of the TERB1 versus TRF1 signals. Quantitation shows that GFP-TERB1 I645F distributes to the wider area compared to WT protein presumably because of its persistent

interaction with TRF1, which relocates to the surrounding area after cap exchange. Mean (red dot), s.d. (red bar), and *P*-values are indicated.

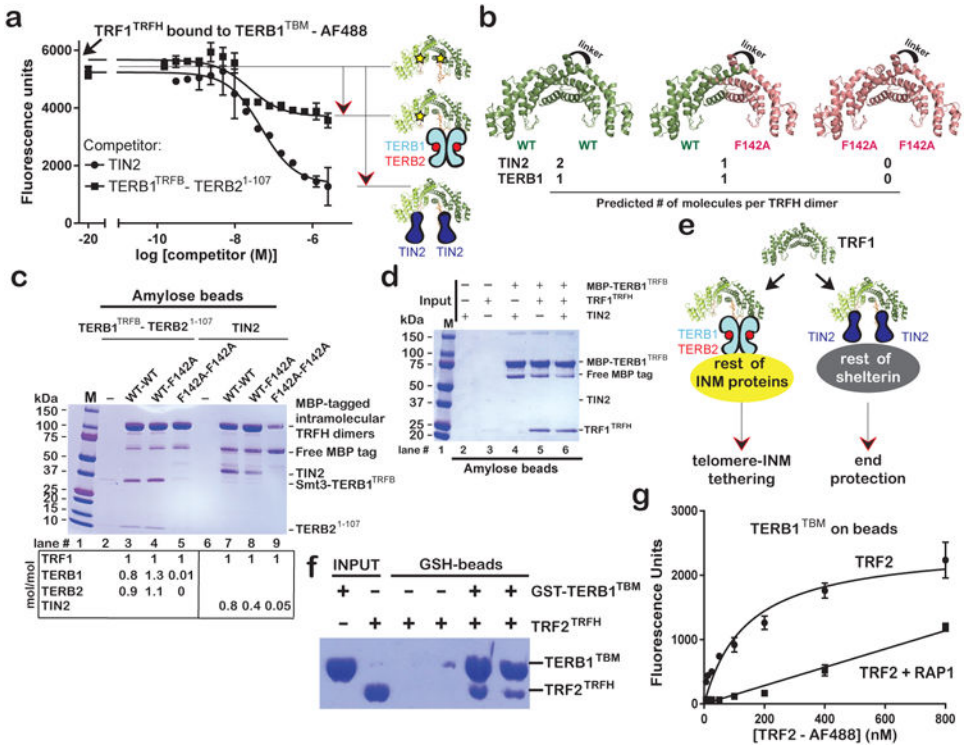

Figure 4. Defining protein complexes involved in telomere tethering versus chromosome end protection

(a) Fluorescence-based competition experiments using Alexa Fluor 488-labeled GST-TERB1^{TBM} pre-bound to biotin-tagged TRF1^{TRFH} on streptavidin beads titrated with varying concentrations of unlabeled full-length TIN2 and TERB1^{TRFB} – TERB2$^{1-107}$ proteins. Mean of technical duplicate is plotted. Error bars indicate s.e.m. The schematics alongside the data represent probable binding stoichiometry. The yellow stars indicate fluorophore-labeled TERB1^{TBM} peptides bound to the TRF1 dimer. Three biological replicates were performed. (b) Strategy for engineering intramolecular homodimers or heterodimers of human TRF1^{TRFH} containing WT and/or F142A sequence connected in tandem by a gly/ser linker; and the predicted number of binding sites for TIN2 and TERB1. (c) Amylose pull down with indicated intramolecular TRF1^{TRFH} dimeric constructs was performed to determine the stoichiometry of binding of TERB1 versus TIN2 for a TRF1 dimer. Quantitation of the coomassie-stained PAGE shown at the bottom was performed by dividing the appropriate band intensities by the molecular weight of the species followed by normalization against the molecular weight-normalized TRF1^{TRFH} dimer signal in that lane. See Supplementary Fig. 6d and e, for replicate data and statistics, respectively. (d) Ternary pull down experiment on amylose resin of MBP-tagged TERB1^{TRFB} – TERB2$^{1-107}$ and TRF1^{TRFH}, and TIN2. Experiment was performed twice. (e) Model showing separate TRF1-containing complexes for protecting chromosome ends and tethering telomeres to the INM during meiosis. (f) GST pull down of TRF2^{TRFH} using GST-TERB1^{TBM} peptide on glutathione (GSH) sepharose beads as bait. Experiment was performed twice. (g) Direct binding curves of biotin-tagged GST-TERB1^{TBM} with Alexa Fluor 488-labeled full-length

TRF2 either in the absence or the presence of Rap1 protein. Mean of technical duplicate is plotted. Error bars indicate s.e.m. Two biological repeats were performed.

Table 1

Data collection and refinement statistics for the TRF1^{TRFH}-TERB1^{TBM} structure (molecular replacement)

	Human TRF1^{TRFH} – human TERB1^{TBM} (PDB code: 5WIR)
Data collection	
Space group	$P6_4$
Cell dimensions	
a, *b*, *c* (Å)	161.72, 161.72, 45.17
α, β, γ, (°)	90.00, 90.00, 120.00
Resolution (Å)	52.94 – 2.10 (2.16 – 2.10) [a]
R_{merge}	11.8 (53.3)
$I/\sigma I$	12.4 (3.8)
Completeness (%)	100 (100)
Redundancy	11.6 (11.3)
Refinement	
Resolution (Å)	46.69 – 2.10 (2.15 – 2.10)
No. reflections	31913
R_{work} / R_{free}	17.90 / 21.04 (19.32 / 22.06)
No. atoms	3778
Protein	3446
Ligand/ion	0
Water	332
B factors	29.37
Protein	34.93
Ligand/ion	N/A
Water	41.44
R.m.s. deviations	
Bond lengths (Å)	0.009
Bond angles (°)	0.993

Table 2
Competition analysis of TRF1 and TRF2 with TERB1 mutants

Relative IC_{50}		
	$TRF1^{TRFH}$	**$TRF2^{TRFH}$**
$TERB1^{TBM}$ WT	**1**	**1**
$TERB1^{TBM}$ I645E	N.D.	2.25 ± 1.0
$TERB1^{TBM}$ I645F	0.3 ± 0.04	2.6 ± 0.64
$TERB1^{TBM}$ L647E	N.D.	N.D.
$TERB1^{TBM}$ T648A	1.2 ± 0.11	0.4 ± 0.07
$TERB1^{TBM}$ T648E	N.D.	N.D.
$TERB1^{TBM}$ P649E	N.D.	N.D.
$TERB1^{TBM}$ R652E	N.D.	1.05 ± 0.32
TIN2-TBM	0.045 ± 0.02	1.15 ± 0.18
$TERB1^{TRFB}$ - $TERB2^{1-107}$ WT	1	1
$TERB1^{TRFB}$ - $TERB2^{1-107}$ I645E	N.D.	0.4 ± 0.07
$TERB1^{TRFB}$ - $TERB2^{1-107}$ I645F	0.45 ± 0.1	0.8 ± 0.0
$TERB1^{TRFB}$ - $TERB2^{1-107}$ L647E	N.D.	N.D.
$TERB1^{TRFB}$ - $TERB2^{1-107}$ P649E	N.D.	N.D.
TERB1-TBM WT	2.1 ± 0.07	0.39 ± 0.03

Mean and s.e.m. of IC_{50} values of indicated TERB1 constructs from fluorescence-based competition experiments done in duplicate normalized to the IC_{50} of the interaction indicated in bold. N.D. indicates the IC_{50} could not be determined because of a lack of competition in the protein concentration range tested (0.6 nM - 10 μM).